THE JOURNAL OF PHYSICAL CHEMISTRY B

Article

Cite This: J. Phys. Chem. B 2018, 122, 6328−6340

pubs.acs.org/JPCB

# Vibronic Wavepackets and Energy Transfer in Cryptophyte Light-Harvesting Complexes

Chanelle C. Jumper,[†,§,∥] Ivo H. M. van Stokkum,[‡,∥] Tihana Mirkovic,[†] and Gregory D. Scholes*[,†,§]

[†]Department of Chemistry, University of Toronto, 80 St. George Street, Toronto, Ontario M5S 3H6, Canada

[‡]LaserLaB, Department of Physics and Astronomy, Vrije Universiteit Amsterdam, De Boelelaan 1081, 1081 HV Amsterdam, The Netherlands

[§]Department of Chemistry, Princeton University, Washington Road, Princeton, New Jersey 08544, United States

Supporting Information

**ABSTRACT:** Determining the key features of high-efficiency photosynthetic energy transfer remains an ongoing task. Recently, there has been evidence for the role of vibronic coherence in linking donor and acceptor states to redistribute oscillator strength for enhanced energy transfer. To gain further insights into the interplay between vibronic wavepackets and energy-transfer dynamics, we systematically compare four structurally related phycobiliproteins from cryptophyte algae by broad-band pump−probe spectroscopy and extend a parametric model based on global analysis to include vibrational wavepacket characterization. The four phycobiliproteins isolated from cryptophyte algae are two "open" structures and two "closed" structures. The closed structures exhibit strong exciton coupling in the central dimer. The dominant energy-transfer pathway occurs on the subpicosecond timescale across the largest energy gap in each of the proteins, from central to peripheral chromophores. All proteins exhibit a strong 1585 $cm^{-1}$ coherent oscillation whose relative amplitude, a measure of vibronic intensity borrowing from resonance between donor and acceptor states, scales with both energy-transfer rates and damping rates. Central exciton splitting may aid in bringing the vibronically linked donor and acceptor states into better resonance resulting in the observed doubled rate in the closed structures. Several excited-state vibrational wavepackets persist on timescales relevant to energy transfer, highlighting the importance of further investigation of the interplay between electronic coupling and nuclear degrees of freedom in studies on high-efficiency photosynthesis.

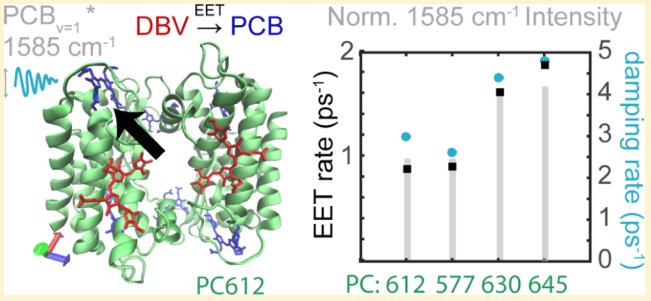


## 1. INTRODUCTION

Photosynthetic energy conversion is initiated by photoexcitation of chromophores that are bound at high concentration in light-harvesting complexes. This excitation energy is conveyed efficiently among the chromophores to a membrane-bound reaction center where charge separation occurs.[1−3] Although theories for adiabatic electronic energy transfer are well developed, the persistence of vibrational coherences in the excited states of protein−chromophore systems has highlighted the potential importance of nuclear motion in connecting donor and acceptor states for efficient energy transfer. Of interest are vibrational coherences that are sustained in the excited state on timescales relevant to energy transfer and/or have mixed exciton-vibrational character.[4−24] In particular, vibronic mixing between donor exciton states and acceptor excited-state vibrations in PC645 has been demonstrated by two-dimensional (2D) electronic spectroscopy and predicts a multiplicative increase in the rate of energy transfer through a redistribution of oscillator strengths affecting the Förster overlap integral.[25] The goal of this work is to measure and fully characterize vibronic coherences and concurrent energy-transfer events in a set of four related light-harvesting complexes from cryptophyte algae to gain insights into the interplay of these dynamics.

Broad-band transient absorption spectroscopy with femtosecond pulses allows energy-transfer dynamics and excited-state vibrations to be monitored simultaneously. This is achieved with excitation pulses having a shorter duration than the vibrational periods and a bandwidth greater than the energy separation between vibrational levels.[26,27] The result is superimposed population and coherence dynamics, and features in these experiments (amplitude and phase profiles) help us to assign vibrational coherence occurring either in the excited or ground state and to assess whether the coherence has mixed exciton-vibrational character. A node in the amplitude, accompanied by a corresponding phase flip, marks the minimum (difference energy) of the electronic potential energy surface that the wavepacket is propagating on.[19,20,28−39] Whether vibrational wavepackets are generated on the ground- or excited-state potential energy surfaces also depends on the

Received: March 18, 2018
Revised: May 8, 2018
Published: May 30, 2018






DOI: 10.1021/acs.jpcb.8b02629
J. Phys. Chem. B 2018, 122, 6328−6340

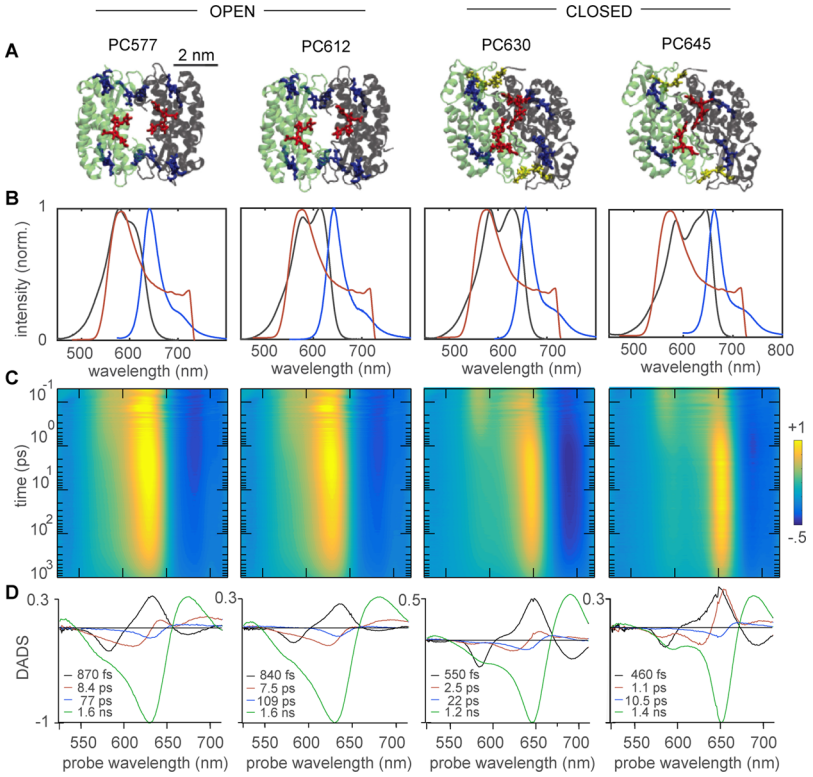


**Figure 1.** (A) Protein structures from PC577, PC612, PC630, and PC645 rendered from X-ray crystal structures. Chromophores are DBV (red), PCB (blue), and MBV (yellow). (B) Normalized absorption (black) and fluorescence (blue) spectra of the proteins and the pulse spectrum (red) used to excite and probe the sample in pump−probe experiments. The pulse spectrum maximum is centered at 580 nm in the region of the high-energy DBV chromophores, present in each of the four phycobiliproteins. The pulse spectrum extends past the red edge of the absorption spectrum of each protein to the excited-state absorption region up to 720 nm. (C) Normalized broad-band transient absorption maps using the excitation and probe pulse from (B) showing comparative movement of energy from the blue side to the red side for each protein. (D) Estimated DADS of each protein with corresponding lifetimes listed in the figure.

properties (spectrum, duration, and chirp) of the exciting pulse[40−45] and ground-state vibrations can be suppressed by a sufficiently short broad-band pulse.[26,27]

Usually, oscillations are analyzed after removal of the population dynamics and the data are Fourier-transformed to the frequency domain to analyze the frequency and phase as a function of probe wavelength or oscillation residuals are analyzed in the time domain at a particular probe wavelength, which can estimate damping times. In both cases, only the signals after the maximum of the IRF are analyzed. To fully characterize vibrational coherences, we will extend a parametric model based on global analysis to include the global analysis of vibrational wavepacket dynamics (damped oscillations), previously applied to PC612.[46] The result is that we are able to simultaneously fit the population and oscillatory dynamics in the entire time domain to investigate the interplay between excited-state vibrations and energy-transfer dynamics. A similar approach of globally analyzing vibrational wavepackets has been taken by Schott et al. for the analysis of trihalide anion photofragmentation products.[47]

Experimentally assessing the influence of vibrational or vibronic coherences is difficult because in intact photosynthetic systems, there are few opportunities for controls or comparisons. Turning on or off a certain feature to evaluate their effect may not be possible. The discovery of four structurally related phycobiliproteins from cryptophyte algae (PC645, PC630, PC612, and PC577) offers a unique opportunity for comparative studies because they have very similar structures and chromophore composition but have differences in excitonic coupling and vibronic signatures. In previous works,[19,20] oscillations were identified through the power spectra of the probe wavelength-integrated pump−probe maps after the removal of decay dynamics. Experiments were performed by parallel polarization between the pump and probe pulses to emphasize vibrational dynamics at the expense of spectral amplitude conservation during energy transfer. In this work, we use magic angle experiments to measure energy transfer and equilibration dynamics in which spectral amplitude may be conserved. Our goal in this work is to systematically compare these four proteins by broad-band pump−probe spectroscopy and fully characterize the resulting vibrational wavepackets (frequencies, intensities, and dephasing times) and energy-transfer dynamics concurrently to reveal additional insights into how energy is steered through these complexes.

Energy-transfer rates and oscillatory signatures will be described for four light-harvesting complexes: phycocyanin 577 (PC577) isolated from the cryptophyte *Hemiselmis pacifica* (CCMP 706), phycocyanin 612 (PC612) isolated from *Hemiselmis virescens* CCAC 1635 B, phycocyanin 630 (PC630) isolated from *Chroomonas* CCAC 1627 B (marine), and phycocyanin 645 (PC645) isolated from *Chroomonas mesostigmatica* CCMP269. PC645 and PC630 are related structures, having the same chromophoric composition and organization composed of three chromophore identities: dihydrobiliverdin (DBV), phycocyanobilin (PCB), and mesobiliverdin (MBV). PC577 and PC612 are also related


DOI: 10.1021/acs.jpcb.8b02629
J. Phys. Chem. B 2018, 122, 6328−6340

structures, having the same chromophoric organization, but differ from PC645 and PC630 by a single amino acid mutation that leads to an open structure and are composed of only DBV and PCB chromophores.[48] The former have strong coupling in the two central dimers, whereas the latter have a separation between these two chromophores, leading to weaker coupling. We obtain population dynamics by fitting decay-associated difference spectra (DADS) and species-associated difference spectra (SADS) using an appropriate compartmental model and obtain oscillatory dynamics by fitting damped oscillation-associated spectra (DOAS) to the data.

## 2. EXPERIMENTAL & ANALYSIS METHODS

**2.1. Sample Preparation.** Phycobiliproteins proteins PC577, PC612, PC630, and PC645 were isolated from cryptophyte algae and purified according to the following procedure. *H. pacifica* (CCMP706) was cultured in the enriched seawater medium, Prov50 (from NCMA), on a 12/12 h dark−light cycle 20 $\mu$E m$^{-2}$ s$^{-1}$ in the growth chamber at 16 °C, whereas *Chroomonas* (CCAC 1627 B, also M1627) was grown under identical conditions but in the L1 medium (also from NCMA). *C. mesostigmatica* (CCMP269) was cultured at room temperature in either K or Prov50 media from NCMA on a 12/12 h dark−light cycle 20 $\mu$E m$^{-2}$ s$^{-1}$. Cells were harvested by centrifugation and were resuspended in 0.1 M sodium phosphate buffer (pH 7.5). Phycocyanin 577 (PC577) was isolated from *H. pacifica* (CCMP706) and phycocyanin 630 (PC630) was obtained from *Chroomonas* (CCAC 1627 B, also M1627), whereas phycocyanin 645 (PC645) was extracted from *C. mesostigmatica* (CCMP269). The water-soluble phycobiliproteins were extracted through freezing and thawing (−20 and 4 °C) in the dark. Further purification steps required centrifugation to remove any impurities following successive ammonium sulfate precipitation (40, 55, and 80%). The final centrifugation at 80% was performed in an ultracentrifuge for 20 min at 35 000 rpm, and the resulting protein pellet was resuspended in 0.050 M phosphate buffer (pH 7.5) for storage at −20 °C. Solutions were prepared in a final concentration of 25 mM phosphate buffer and protein at an optical density of 0.15/mm.

**2.2. Steady-State Spectroscopy.** Room-temperature absorption spectra were recorded using a Varian Cary 6000i UV−vis spectrometer with a resolution of 1 nm. Fluorescence emission spectra were recorded on a Fluorolog-3 (Horiba) spectrometer in a 90° mode, with a xenon arc light source and an R928 photomultiplier tube.

**2.3. Pump−Probe Experiments.** The transient absorption spectrometer setup is described in detail elsewhere.[19] Broadband pulses were generated from a commercial 5 kHz Ti:sapphire laser amplifier (Spectra-Physics, Spitfire) pumped into a home-built noncollinear optical parametric amplifier. The spectrum was tuned centrally to 580 nm with an asymmetric Lorentzian extending past 720 nm, overlapping well with the entire PC577, PC612, PC630, and PC645 absorption spectra and strongly exciting the higher-energy DBV chromophores in each case (Figure 1B). The pulse was compressed with a folded grating compressor and a prism compressor (one prism and a retroreflector) to ≈18 fs as determined by polarization-gated frequency-resolved optical gating. This pulse has a duration shorter than the vibrational periods probed up to 1850 cm$^{-1}$ and a bandwidth (4000 cm$^{-1}$ full width at half-maximum) exceeding those vibrational level splittings. The pulse was split into identical pump, probe, and reference beams with a 1° UV-fused silica wedge. The reference and probe beams were those reflected from the front and back surfaces of the wedge with less than 1% total intensity, whereas the transmitted beam was used for the pump. The probe beam was directed through the sample and was dispersed and focused onto a 1.25 kHz charge-coupled device detector. The sample flowed through an ice bath and a 1 mm quartz cuvette at a rate of 1 mL/min with a peristaltic pump. A translation stage in the pump path was used to achieve the time delay between the pump and probe. The sample was pumped at 6 nJ/pulse and successive sets of four probe pulses with the pump blocked and unblocked were recorded. The pump and probe beam had magic angle polarization and were focused onto 1/e beam diameters of 40 and 15 $\mu$m, respectively. The probe intensity was balanced by the reference beam intensity as measured on a photodiode to eliminate influences from laser fluctuations during the experiment. The $\Delta I/I$ value was then determined by

$$I_{\text{balanced}} = \left(\frac{I_p}{S_p} - \frac{I_u}{S_u}\right)/\left(\frac{I_u}{S_u}\right)$$

where $I_p$ and $I_u$ are the intensities of the pumped and unpumped probe signals, respectively, and $S_p$ and $S_u$ are the corresponding intensities of the photodiode signals. The values entered into this equation are the sum of the four-pulse sequence and averaged for 300 consecutive cycles. This process was repeated for each delay time following a nonlinear range from −5 ps to 1 ns and repeated five times.

**2.4. Global & Target Analysis.** The time-resolved spectroscopy data of multichromophoric systems contain an overwhelming wealth of information, which describe the spectral evolution of electronically excited states. The overall observable spectroscopic changes are a combination of all microscopic underlying processes. We describe the data by a parametric model, employing global and target analysis[49−51] of the time-dependent spectral evolution. The goal of global analysis is the simultaneous analysis of all measurements giving fits of the data with a sufficient number of exponential decays: $c_l(t) = \exp(-k_l t)$. The probe wavelength-dependent amplitude of the exponential decays used to globally fit the entire data set constitutes DADS.[51] The DADS read-out the loss or gain in signal with a certain lifetime as a function of the probe wavelengths. The number of DADS equals the number of decay rates necessary to fit the complete data set and the number of resolvable compartments. In target analysis, we determine the microscopic rate constants between interacting compartments (electronically excited states in this case) in the system in a K-matrix, whose eigenvalues give rise to decay rates of the global fits. The time-resolved spectra TRS($t$,$\lambda$) are described by a parametrized superposition model

$$\text{TRS}(t, \lambda) = \sum_{l=1}^{N_{\text{states}}} c_l^S(t, k)\text{SADS}_l(\lambda)$$

where the spectral properties of the compartments are the species-associated difference spectra (SADS$_l(\lambda)$) and their populations are $c_l^S(t,k)$ (superscript S stands for species) with kinetic parameters $k$. The details and all mathematical relationships and derivations can be found in van Stokkum et al.[49,50]

**2.5. Global Oscillation Analysis.** The evolution of the vibrationally excited state wavepackets created by a short laser pulse is described with a superposition of damped oscillations.


DOI: 10.1021/acs.jpcb.8b02629
J. Phys. Chem. B 2018, 122, 6328−6340

The probe wavelength-dependent amplitude of a damped oscillation $\cos(\omega_n t)\exp(-\gamma_n t)$ constitutes a damped oscillation-associated spectrum $\mathrm{DOAS}_n(\lambda)$ with an accompanying phase characteristic $\varphi_n(\lambda)$. Assuming the independent evolution of the electronic and vibrational degrees of freedom by the Born–Oppenheimer approximation, a superposition of the electronic and vibrational contributions to $\mathrm{TRS}(t,\lambda)$ can be described as

$$\mathrm{TRS}(t,\lambda) = \sum_{l=1}^{N_{\mathrm{states}}} c_l^S(t', k)\mathrm{SADS}_l(\lambda) + \sum_{n=1}^{N_{\mathrm{osc}}} \mathrm{DOAS}_n(\lambda)\cos(\omega_n t' - \varphi_n(\lambda))\exp(-\gamma_n t')$$

where $t'$ indicates that the instrument response function has not yet been included. The number of vibrationally excited states $N_{\mathrm{osc}}$ is determined, and we estimate their parameters, the eigenfrequency $\omega_n$ and damping rate $\gamma_n$, and the $\mathrm{DOAS}_n(\lambda)$ and $\varphi_n(\lambda)$. The number of vibrationally excited states that can be reliably resolved depends upon the signal-to-noise ratio of the measurements $\mathrm{TRS}(t,\lambda)$. The applicability of the methodology was published in ref 46 for PC612 and here it is applied to resolve the DADS, SADS, and DOAS for the set of four phycobiliproteins.

**2.6. Computation of Spectral Densities.** Experimental spectral densities were generated for each protein from the DOAS data (Supporting Information Table S1) as a sum of Lorentzian lines according to

$$S(\omega) = \sum_{n=1}^{N_{\mathrm{osc}}} A_n \frac{\Gamma_n}{(\omega - \omega_n)^2 + \Gamma_n^2}$$

where $\omega_n$ is the center frequency of the $\mathrm{DOAS}_n$, $\Gamma_n$ dephasing rates were translated from the fitted dephasing rates $\gamma_n$ by the time bandwidth product ($\Delta t \Delta \upsilon = 0.142$), and each peak is scaled by $A_n = \mathrm{area}/\gamma_n$.

## 3. RESULTS AND DISCUSSION

**3.1. Structures and Absorption.** The protein structures scaffold and organize the chromophore units in their optimal configuration for their function in light harvesting. We first present the structures, chromophore organization, and energetic ordering of the four phycobiliproteins being compared in this work. The X-ray crystal structures of PC577, PC612, PC630, and PC645 are shown in Figure 1A, including the line structures of the embedded chromophores (DBV, PCB, and MBV) as labeled. In the open structures (PC577 and PC612), the central DBVs (red) are ≈2 nm apart, and in the closed structures (PC630 and PC645), they are ≈0.5 nm apart and form a molecular excitonic dimer.

The corresponding steady-state absorption spectra for the four proteins are shown in Figure 1B (in black) and show broad features that are composed of overlapping contributions from the different chromophores, their homogeneous and inhomogeneous line widths, vibrational sub-bands, and excitonic coupling. The site energies of the individual chromophores must be obtained through quantum mechanical modeling and/or optimized fits to the data. For PC645, the chromophores contributing to the high-energy part of the spectrum have been determined to be DBV molecules (≈580 nm) and those in the lowest energy part of the spectrum are the PCB molecules (≈635–650 nm).[25,52−55] The red-most PCB molecules are the PCB 82C and PCB 82D, with PCB 158C and PCB 158D slightly higher up on the energy ladder. There is an additional MBV molecule absorbing in the middle of the spectrum (≈610–622 nm), present only in the closed structures. It has been shown that isolated phycobiliproteins fluoresce from a single terminal emitter PCB 82C, suggesting that energy is funneled to a single chromophore in the energy funnel. The emission spectra are depicted in blue in Figure 1B.

A single residue insertion is responsible for the structural changes between the four proteins, which primarily separates the central dimer. The chromophores are otherwise in similar protein environments and are expected to follow the same energetic ordering with DBVs at the high-energy end and PCBs at the low-energy end. The closed structures exhibit a larger range of absorption energies, with the PCB region shifted farther to the red than the open structures. The same broadband pump pulse was used for time-resolved experiments and is shown in red in Figure 1B. This pulse excites most strongly the DBV chromophores at 580 nm, covers the entire absorption spectrum, and has amplitude out to 720 nm, which can capture excited-state absorption signals.

**3.2. Population Dynamics.** Figure 1C shows the broadband pump–probe spectra for all four proteins over a nonlinear time axis extending to 1 ns. In contrast to narrow-band transient absorption spectroscopy, commonly used to analyze population dynamics, all chromophores are excited at once with the pump pulse in these experiments. The spectra display bleach and stimulated emission features across the entire absorption region of each light-harvesting complex and excited-state absorption features mainly to the red of this wavelength range. Equilibration of the excitation energy occurs downhill in energy until the final emission from the terminal chromophore. At first inspection of the spectra, the movement of excitation appears to be dominated by decay from the high-energy end (indicated by the negative amplitudes of the black and red DADS) and corresponding growth at the lowest energy end (indicated by the positive amplitudes of the black and red DADS), especially for the two closed structures on the right. To further decompose the kinetics of the energy-transfer events, we performed global and target analysis of the population dynamics.

Four lifetimes were required to fit the data set and the DADS are shown in Figure 1D with estimated lifetimes listed in the figure and in Table 1. The DADS plot the amplitude of the global exponentials used to fit the complete data set as a function of probe wavelength, where negative amplitude indicates an exponential decay of bleaching and stimulated emission signals and positive amplitude indicates an exponential growth thereof. The black DADS correspond to the fastest observable dynamics in the complex and show the simultaneous exponential decay in the blue region, where the donor DBV chromophores are located, and corresponding exponential

**Table 1. Estimated Lifetimes for the Four Proteins (ps) Corresponding to the DADS in Figure 1D[a]**

| | | open structures | | closed structures | |
|---|---|---|---|---|---|
| | | PC577 | PC612 | PC630 | PC645 |
| $\tau 1$ | black | 0.87 | 0.84 | 0.55 | 0.46 |
| $\tau 2$ | red | 8.4 | 7.5 | 2.5 | 1.1 |
| $\tau 3$ | blue | 77 | 109 | 22 | 10.5 |
| $\tau 4$ | green | 1648 | 1569 | 1216 | 1412 |

[a]Errors in fits are up to 10%.



DOI: 10.1021/acs.jpcb.8b02629
J. Phys. Chem. B 2018, 122, 6328–6340

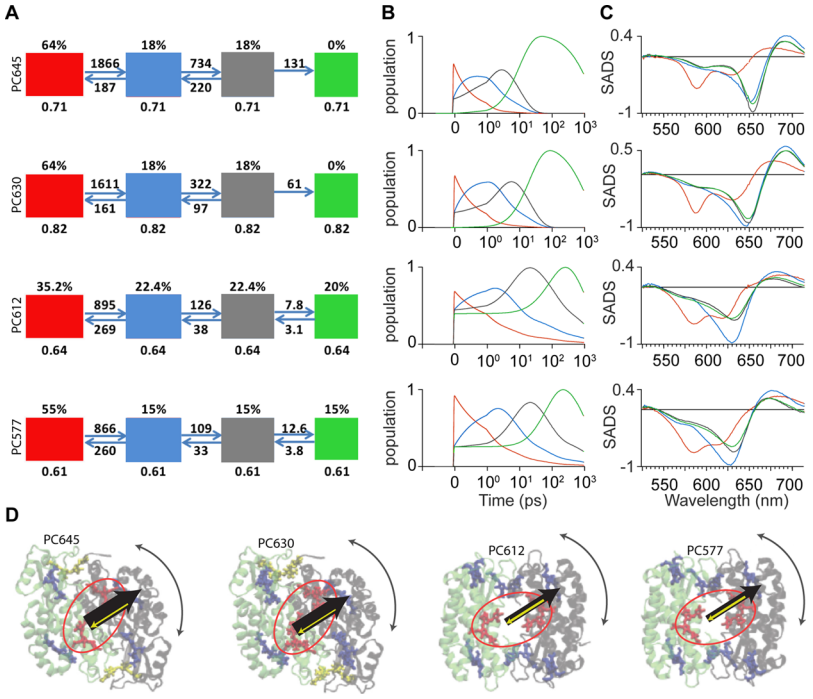


**Figure 2.** Target analysis of PC577, PC612, PC630, and PC645. (A) Kinetic scheme with microscopic rate constants (in $ns^{-1}$). Input fractions are on top of each of the four compartments. (B) Population profiles of the four species, note that the time axis is linear until 1 ps (after the maximum of the IRF) and logarithmic thereafter. (C) Estimated SADS. (D) Schematic of energy-transfer pathways in the four proteins. The first compartment represents the central DBV donors (red) and the second compartment represents PCB acceptors (blue). Equilibration between the first and second compartment are indicated by black arrows (forward rate) and yellow arrows (reverse rate). The thickness of these arrows is in proportion to the transfer rates for each protein. Final equilibration between the PCBs is indicated by gray double-headed arrows and correspond to unresolved compartments in gray and green.

growth in the red region to the PCB molecules. This indicates almost conservative energy transfer between the DBV and PCB chromophores in these regions. Surprisingly, this fast and most efficient stage of energy transfer spans nearly the largest energy gap in each of the systems.

The second lifetime (red DADS) corresponds to equilibration between chromophores farthest to the red. The third lifetime in the open structures on the order of 100 ps shows a nonconservative decay of bleach plus stimulated emission at ≈640 nm and excited-state absorption at ≈655 nm and is attributed to annihilation. Specifically, there is evidence that these annihilations are due to the presence of long-lived triplet states present on the protein in between probe pulses.[46] The fourth lifetime corresponds to relaxation of the final excited state to the ground state on the nanosecond timescale, in agreement with the known fluorescent lifetimes.[56,57]

Target analysis was performed to estimate microscopic rate constants based on a compartmental model that allows equilibration between the first three compartments followed by decay from the final state: A ↔ B ↔ C ↔ D→. The resulting rate constants between compartments are shown in Figure 2A with the corresponding population growths and decays of each species in Figure 2B and the estimated SADS in Figure 2C. Although there are eight chromophores in each protein and potentially numerous energy-transfer pathways, we can only resolve the microscopic rate constants for the number of compartments that equals the number of global lifetimes. Note that initially 55, 35, 64, and 64% of the excited states are in the red compartment, corresponding to DBV. In the open structures, the remainder is distributed (almost) evenly over the blue, gray, and green compartments, corresponding to PCB. In the closed structures, the remainder is distributed evenly over the blue and gray compartments, corresponding to PCB and MBV, respectively.

By inspection of the SADS, we see that the energy-transfer step between the first two compartments (red to blue) spans the largest energy gap in the complex. The DBV SADS show minima at ≈585 and 620−630 nm because of bleaching and stimulated emission.[58] In agreement with the interpretation of the red DADS, the maxima of the blue SADS are nearest to the red-most species in each complex, indicating that the largest energy gap is bridged by the first and fastest energy-transfer step (excluding the unresolved DBV exciton relaxation; see below). This jump occurs twice as fast in the closed protein structures as in the open protein structures. The second SADS resemble a PCB absorption spectrum with a shoulder overlapping the DBV region, where $PCB_{v=1}$ would overlap for a 1585 $cm^{-1}$ vibronic mode,[25] which we will discuss in the final section. The final equilibration steps that are between the red-most chromophores occur on the picosecond timescale (7.5−22 ps) across a relatively flat energetic landscape. This final step was previously reported by Mirkovic et al. to be ≈15 ps in PC645, within this range, and is faster than computational quantum chemical predictions of 40 ps.[52] Although with excitation at 645 and 662 nm of PC645, Marin et al. found a 46 ps component and assigned this to the final hop.[53] This longer component is not observed in our broad-band excitation experiments and the red-most SADS align with the fluorescence emission (see Supporting Information Figures S6−S9B), suggesting that equilibration is complete on a faster timescale. Recall that we have assigned the ≈100 ps component in the open structures (blue DADS in Figure 1D) to annihilation.



DOI: 10.1021/acs.jpcb.8b02629
J. Phys. Chem. B 2018, 122, 6328−6340

The overall resolved kinetic scheme is illustrated in Figure 2D, which highlights the equilibration between the central high-energy DBV chromophores and low-energy acceptor PCB chromophore(s) (black arrows represent forward rate and yellow arrows represent reverse rate, with their thickness in proportion to the rate constants). Final equilibration between the lowest-energy PCB chromophores is shown with gray double-headed arrows. The equilibria in the kinetic schemes in Figure 2 correspond to free-energy differences. In the closed structures, these are 480 and 250 $cm^{-1}$, and in the open structures, these are three times 250 $cm^{-1}$. Thus, the total free energy that has to be dissipated during the equilibration is about 750 $cm^{-1}$. This roughly corresponds to the energy difference between the stimulated emission maxima of the DBV and the final PCB.

The key features contributing to efficient energy transfer employed by nature have long been sought after. In an effort to determine accurate energy-transfer rates and pathways in phycobiliproteins, for example, narrow-band pump−probe spectroscopy has been used along with global and target analysis with the goals of generating the "complete picture" of the energy-transfer funnel. For example, Marin et al. studied isolated PC645 and by initiating single energy-transfer pathways by exciting individual chromophores with a narrow-band pulse, generated a step-wise energy funnel picture from high to low energy across a number of timescales. However, in intact cells (Rhodomonas CS24 comprising PC645), it has been shown that energy transfer from the phycobiliproteins to the chlorophyll acceptors in the thylakoid membrane proteins can occur from any of the peripheral bilin chromophores.[54,55]

Although the energy ladder in these proteins represents a stepwise ladder from high to low energy, the stepwise transfer down the ladder is not necessarily the most efficient or chosen pathway. Here, we find that the fastest (and most efficient) energy-transfer step leaps nearly the entire energy ladder on the subpicosecond timescale. This is in agreement with Marin et al., which confirmed that DBV transferred directly to peripheral PCB rather than the intermediate MBV molecules.[53] In accordance, it was also suggested that MBV molecules independently funnel energy to the peripheral chromophores in a concerted pathway.[53,56] Because the overall role of the protein as an antenna is to down-convert energy for the transfer to lower-energy chlorophylls, it is possible that the optimized route will take excitation energy in the most direct pathway to the final emitters, regardless of which chromophore is excited.

The presence of this dominant energy-transfer pathway was also shown by Dean et al. who studied the ultrafast energy transfer and coherence dynamics by two-dimensional electronic spectroscopy.[25] By analyzing the 2D amplitude patterns, they found evidence of a vibronic coupling mechanism that bridges the donor DBV and acceptor PCB by a ≈1600 $cm^{-1}$ mode. This vibronic coupling is thought to redistribute oscillator strength in the donor/acceptor pair resulting in an enhancement to the Förster energy-transfer rate through modification of the spectral overlap integral. In the next section, we will discuss the application of a new method for time-domain global analysis fitting of coherence dynamics, which will allow us to later analyze the 1585 $cm^{-1}$ mode, as it relates to energy-transfer rates in the four complexes.

Finally, equilibration between the central dimer exciton states was not resolved, but because the complex rapidly distributes excitation energy in the DBV region to the lower-energy PCBs (sub-ps), it is most likely that internal conversion between the high- and low-energy exciton states occurs on a much faster timescale. In agreement, Marin et al. estimated this timescale to be <80 fs based on pump−probe anisotropy signals, though the actual relaxation was unresolved.[53] These estimates are in contrast with previous fluorescence studies that assigned 2 ps components to DBV exciton relaxation,[56] though later this 2 ps component was observed and assigned to transfer between species in the red.[55] Indeed, facilitated by shorter pulse duration and experimental advances, ultrafast internal conversion between exciton states (≤100 fs timescale) has been observed in a growing body of reports.[30,59−73] This motivated our previous work on elucidating exciton dynamics in an isolated strongly coupled dimer.[74] There, we observed a <50 fs relaxation between exciton states, in contradiction to the 2 ps relaxation predicted by stochastic coupling to the bath, highlighting additionally the importance of intramolecular degrees of freedom in the transfer of energy. Next, we will analyze the vibrational wavepackets that accompany the population dynamics in the four phycobiliproteins and focus on their relationship to the first subpicosecond energy-transfer step.

**3.3. Coherence Dynamics.** The transient absorption spectra are rich with oscillatory features in the first ≈1 ps (Supporting Information Figures S1−S5), indicative of vibrations which are strongly coupled to the electronic transition via the Franck−Condon mechanism. One of the common ways of determining the oscillatory frequencies present in the data is to subtract fits of the population dynamics and analyze the residuals by Fourier transform to generate transient absorption oscillation spectra. Figure 3 shows the resulting Fourier transform maps of the transient absorption spectra (and probe wavelength-integrated spectra) after removal of biexponential decays from each probe wavelength for the linear sampling range of the experiment between 30 fs and 2 ps (3 fs steps). The number of vibrational modes that are resolved in the spectra depends on the pulse duration and bandwidth, where pulses with duration shorter

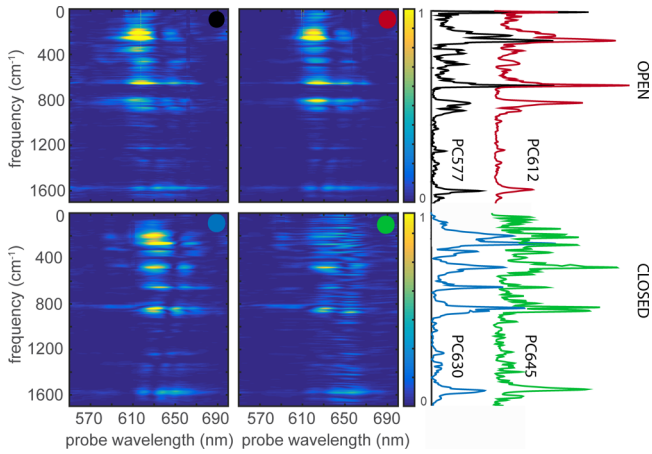


**Figure 3.** Wavelength-dependent Fourier transform map of residual oscillations after removal of fitted population dynamics from pump−probe spectra labeled with colored circles: PC577 (black), PC612 (red), PC630 (blue), and PC645 (green). Amplitudes refer to oscillations at a given frequency in each time trace taken at the probe wavelength. Corresponding probe wavelength-integrated power spectra for the four phycobiliproteins are shown to the right of the Fourier transform maps.



DOI: 10.1021/acs.jpcb.8b02629
J. Phys. Chem. B 2018, 122, 6328−6340

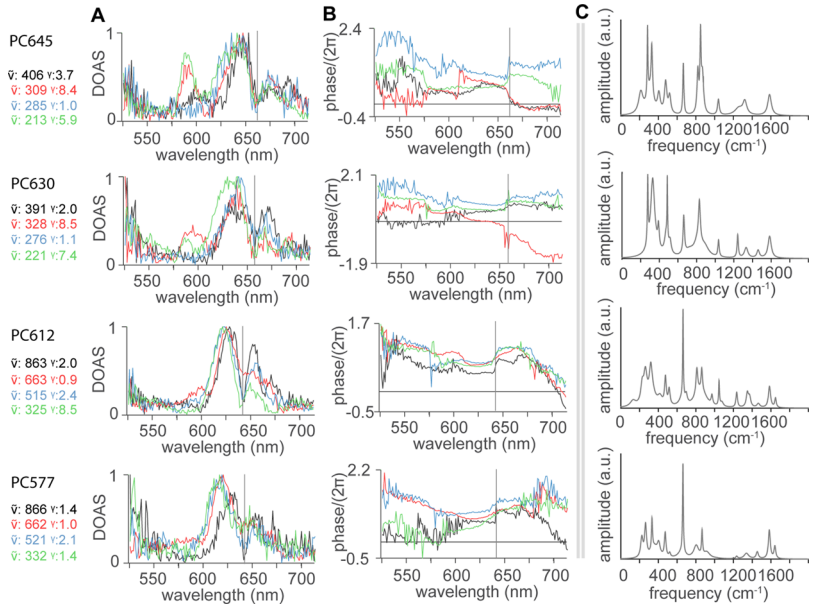


**Figure 4.** Selected oscillation profiles from time-domain global fits for each of the four proteins as labeled. (A) Estimated normalized DOAS corresponding to the frequencies (in $cm^{-1}$) and damping rates (in $ps^{-1}$) color-coded in the legend. (B) Estimated phase profiles of the DOAS. The gray vertical lines indicate dominant nodes in the DOAS and corresponding phases near the fluorescence emission wavelength of each protein at 640 nm (PC577), 641 nm (PC612), 656 nm (PC630), and 661 nm (PC645). (C) Complete "spectral densities" of the four proteins each composed of a sum of Lorentzian lines with center frequency $\tilde{\upsilon}$ and $\gamma$ values from Supporting Information Table S1.

than the vibrational period are required to sample a particular mode and the bandwidth must be wider than the energetic spacing between the levels. The amplitude of a particular vibration must also be greater than the noise fluctuations in the data points. The reproducibility and signal-to-noise of the resolved oscillations detected with the spectrometer are excellent[19] and analyzed in detail in relation to the DOAS fitting method in our previous work.[46]

Using this approach, Arpin et al. applied Gaussian fits to the integrated transient absorption oscillation spectra and resolved between 7 and 8 modes below 1000 $cm^{-1}$ for the four proteins.[20] Using the Fourier transform data to seed, oscillations can be fit in the time domain at particular probe wavelengths to estimate dephasing times. McClure et al. determined the dephasing times for eight oscillations in PC577 at a specific probe wavelength of 616 nm.[19] Because of improvements in our pulse duration, we were able to resolve higher-frequency modes than previously possible in our studies on these proteins, where oscillations above 1000 $cm^{-1}$ were not sampled.

In the impulsive limit of excitation, it is expected that the vibrations are launching in the electronic excited state. Furthermore, there is a distinct region near the emission wavelength of each protein where the amplitude of the oscillations goes to zero. This is indicative of the minimum of the potential energy surface where there is maximum destructive interference in the collection of oscillatory signals probed with a broad bandwidth pulse.[33−40] Analyzing the amplitude and phase characteristics,[39,75−80] these vibrational wavepackets have been assigned to the excited state for the proteins of this study in a previous analysis and compared with femtosecond-stimulated Raman spectroscopic data.[19,20,29] It is difficult from this method to obtain information on the exact amplitudes, dephasing times, and phase profiles of particular coherences because there are many overlapping contributions. To more accurately determine amplitude and phase information and dephasing times, we perform a global analysis of the complete data using damped oscillations.

It is desirable to monitor the population dynamics and coherence dynamics simultaneously, allowing the full characterization of vibrational coherences including amplitude and phase as a function of probe wavelength and dephasing times for each coherence. We developed a fitting method that extends the global fits of population dynamics to include the oscillatory dynamics. The result is the DOAS, which are analogous to the DADS. These plots give the amplitude for a given oscillation, of only a specific dephasing time, across the probe wavelength and we show a range of DOAS for the proteins PC577, PC612, PC630, and PC645 in Figure 4A. The complete set of DOAS for each protein can be found in Supporting Information Figures S6−S9. This method resolves many more oscillations than were possible in the transient absorption oscillation spectra and the list of identified oscillations for all four proteins, with their respective dephasing parameters and spectral areas (scaled by dephasing time, $\gamma_n$) are listed in Supporting Information Table 1. The data in this table are summarized in the spectral density plots presented in Figure 4C, which are in good qualitative agreement with the probe wavelength-integrated power spectra presented in Figure 3B.

The details of the global fitting have been reported.[46] In Table S1, we report the estimated standard errors of the estimated parameters. The estimated precision of the parameters is very high, thanks to the very high quality of the data which possess an excellent signal-to-noise ratio (Figures S1−S4). We simultaneously describe nearly 1000 time-gated spectra (each of 162 wavelengths) with a limited set of only 24 DOAS (with two parameters each, the eigenfrequency $\omega_n$ and damping rate $\gamma_n$). Thus, from the nearly 1000 time-gated spectra, we estimated 24 × 2 = 48 DOAS parameters. This is a huge variance reduction, resulting in precisely estimated DOAS parameters. In addition, the analysis of multiple experiments (typically two or three) results in a further variance reduction


DOI: 10.1021/acs.jpcb.8b02629
J. Phys. Chem. B 2018, 122, 6328−6340

by $\sqrt{2}$ or $\sqrt{3}$. This is in contrast to, for example, a discrete Fourier transform, where the amount of "parameters" (the Fourier coefficients) is huge, and smoothing techniques are needed to arrive at interpretable spectra. Regarding the uniqueness of the solution, we employ Ockham's razor (which is a generally accepted modeling principle) and choose the minimal model that describes the data up to the noise level. Again, this noise level is well defined because we simultaneously fit multiple experiments (typically two or three). DOAS are only included in the model when they significantly reduce the root-mean-square error of the fit and are described by precisely estimated parameters $\omega_n$ and $\gamma_n$.

The DOAS resolve clear nodes in the amplitude similar to those resolved in the transient absorption oscillation maps in Figure 3. The phase associated with each DOAS can be seen in column B of Figure 4. In a broad-band experiment, wavepacket destructive interference is at a maximum at the bottom of the potential energy well. In the DOAS, this manifests as nodes at the minimum of the difference energy between the potential energy surface of their propagation and that of the state involved in the probed electronic transition. The nodes resolved in Figure 4 (indicated by gray vertical lines) are predominantly present at the difference energy between the ground- and excited-state potential energy surfaces of the terminally emitting chromophore for each protein (fluorescence emission wavelength), indicating propagation on the excited-state potential energy surface after the excited states have equilibrated.[81] The fluorescence maxima (from Figure 1) are 640 nm for PC577, 641 nm for PC612, 656 nm for PC630, and 662 nm for PC645. Excited-state vibrations can additionally be identified by oscillatory signals in the stimulated emission or excited-state absorption as the system evolves.

In the wavelength-dependent Fourier transform map of a multichromophore complex, overlapping amplitude from chromophores to the blue obscures the expected nodes for oscillations belonging to intermediate chromophores. Furthermore, the likelihood of resolving a node depends on the duration of wavepacket propagation, which also relies on how long the system remains in a particular excited state as it evolves (transfer energy to other states). Because the system spends more experimental time in the final acceptor excited state, nodes are most clearly resolved in the Fourier transform oscillation maps belonging to this state. In contrast, the DOAS were able to resolve nodal patterns to the blue of the terminal emitter. In Figure 5, two special frequencies are highlighted, which are present in all four proteins, that is, the ≈660 and the 1585 $cm^{-1}$ modes. The 1585 $cm^{-1}$ mode exhibits nodes in the DOAS oscillation amplitudes near 625−630 nm as labeled by the gray bars in Figure 5A. Correlating bands in the DOAS with the SADS from Figure 2 suggests that the ≈1585 $cm^{-1}$ vibrational modes are related to excited PCB states to the blue of the terminal emitters. The ≈660 $cm^{-1}$ modes exhibit nodes in the DOAS oscillation amplitudes at the energies of the corresponding fluorescence emissions and to the blue of these in the closed structures.

The DOAS result from all eight chromophores present in the complex. As explained above, predominantly the DBV, but also the other chromophores are initially excited. Thus, the DOAS method resolves the IVR properties of the pigments and reveals a number of potential PCB-accepting modes which may aid in the down-conversion of energy after transfer from DBV to PCB.[82] The overall vibrational dephasing times, globally fit in the time domain by the DOAS method, result from a

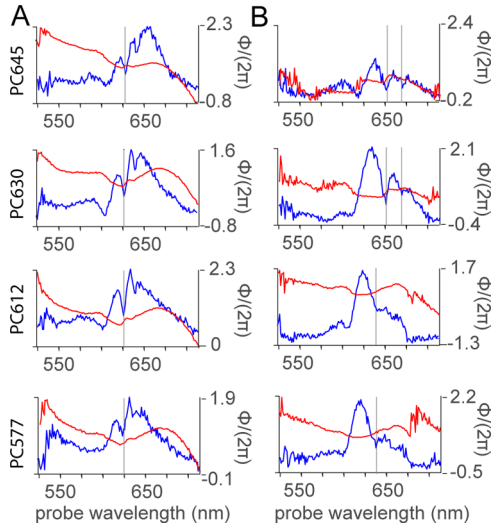


**Figure 5.** Oscillation profiles for the (A) ≈1585 and (B) ≈660 $cm^{-1}$ mode from time-domain global fits for each of the four proteins as labeled on the left. In blue: estimated DOAS. In red: estimated phase profiles of the DOAS. In (A), the gray vertical lines indicate dominant nodes with corresponding phase flips at 628.5 nm (PC645), 628.5 nm (PC630), 626.5 nm (PC612), and 625 nm (PC577) for 1585 $cm^{-1}$. In (B), the gray vertical lines indicate dominant nodes near the fluorescence emission wavelength of each protein (as in Figure 4) and to the blue of these in the closed structures.

combination of pure dephasing, population relaxation of the vibrational levels involved in the coherence, and population relaxation accompanying energy transfer.[83,84] The next section will discuss the dephasing times compared to the lifetimes of the first energy-transfer jump in the protein complexes.

**3.4. Population Versus Coherence Timescales.** The method of simultaneously resolving population and coherence dynamics presented in this work allows us to compare their relative timescales. The dephasing lifetimes (Supporting Information Table S1) for the wide variety of oscillations range from around 100 fs to over 1 ps. As discussed in the previous section, the amplitude and phase profiles for most of the oscillations detected in the pump−probe spectra show very similar patterns, consistent with vibrations occurring in the excited state. Vibrational motion occurs in the excited states on the same timescale as energy transfer is of interest because it indicates energy transfer could be occurring outside the vibrationally relaxed Förster regime.[85] Figure 6A highlights a comparison of a few dominant oscillatory modes, having amplitude and phase profiles indicative of propagation in the excited state (Supporting Information Figures S6−S9), to the lifetime of the first energy-transfer event in each protein.

Using resonance Raman data from PCB-containing proteins, some of the vibrational normal modes can be assigned.[86,87] The ≈660 and ≈1585 $cm^{-1}$ vibrational modes are dominantly present in all four proteins in terms of the areas/$\gamma_n$ of their DOAS and by the relatively long-lived endurance of over 200 fs dephasing lifetimes. The 1585 $cm^{-1}$ mode is in the C═N stretching region of vibrational spectra. The open structures have a dominant mode at ≈1235 $cm^{-1}$ (CH/NH bending and C−C/C−N stretching region) with a dephasing lifetime of over 400 fs. The closed structures show a low-frequency mode at ≈280 $cm^{-1}$ with a dephasing time lasting longer than the first energy-transfer event. Interestingly, the observed dephasing times for the ≈660 and ≈1585 $cm^{-1}$ vibrational modes


DOI: 10.1021/acs.jpcb.8b02629
J. Phys. Chem. B 2018, 122, 6328−6340

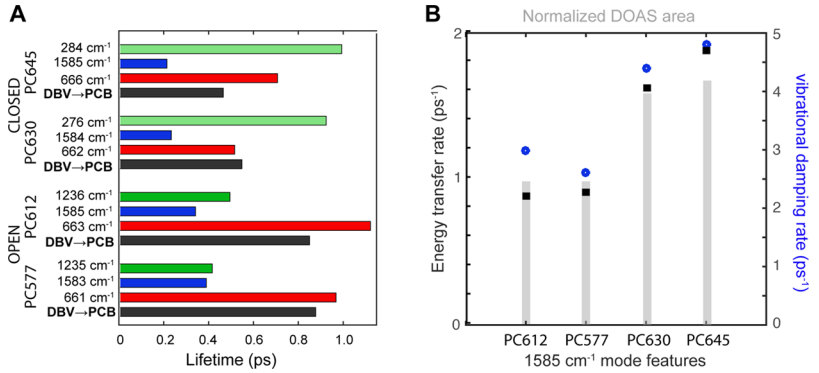


**Figure 6.** Comparison of the equilibration timescales for the first energy-transfer event and (selected) dominant long-lived excited state vibrations in each protein, as labeled. (A) Black bars represent the equilibration lifetime for the dominant energy-transfer pathway between DBV donor and PCB acceptor. The red and blue bars, respectively, represent the damping times for the ≈660 and ≈1585 $cm^{-1}$ vibrational modes, which are present in all four proteins. The dark green bars represent the damping times for the ≈1235 $cm^{-1}$ vibrational mode present in the open structures. The light green bars represent the damping times for the ≈280 $cm^{-1}$ vibrational mode present in the closed structures. (B) Comparison of the downhill microscopic energy-transfer rates (black squares) for the four proteins PC612, PC577, PC630, and PC645 and the 1585 $cm^{-1}$ oscillatory mode feature that bridges the $PCB_{v=1}$ acceptor to the $DBV^-$ donor. In blue is the vibrational damping rate in $ps^{-1}$, and the gray bars show the relative amplitudes of the area/$\gamma_n$ of the DOAS normalized to the 660 $cm^{-1}$ oscillatory mode, also present in all four proteins.

correlate with energy-transfer timescales across the four proteins, though the 1585 $cm^{-1}$ mode is damped far before energy transfer is complete. It is not clear if and how coherent excited-state vibrations affect energy transfer.

Vibrational coherence has previously been reported in the excited states of a variety of photosynthetic systems (including low-frequency modes) found in the donor excited state of the purple bacteria reaction center,[34,80,84,88−91] core light-harvesting antenna (LH1),[90,92,93] B820 unit,[94,95] bacteriochlorophyll *a*,[96] peripheral light-harvesting antenna (LH2),[90,97] chlorosome from green bacteria,[98] Fenna−Matthews−Olson complex,[99−103] and blue copper proteins.[104] Once treated as a simple thermal bath with a smooth spectral density, discrete intramolecular vibrational modes have additionally become apparent as distinct peaks in the spectral densities obtained from quantum mechanical and molecular dynamics simulations,[82,105−107] though the exact mechanisms by which they may contribute to energy transfer are not well understood. The DOAS method presented in this work characterizes the experimental spectral density and is a step toward uncovering the role of specific vibrations in energy-transfer dynamics.

The presence of coherent vibrations on the timescale of energy transfer suggests that there could be a time-dependent modulation of the orientation and spatial separation of chromophores that are key determinants of energy-transfer rates and efficiencies. A Förster-type description of energy transfer is one that occurs from vibrationally relaxed excited states and the maintenance of long-lived vibrational coherence in the participating states indicates that this description is not complete.[85] Coherence across more than one molecule could also be a way to wire the molecules together through overlap or matching of their vibrational phase spaces. In the reaction center, vibronic coherence has been more recently proposed to enhance transport between energetically isolated states by bringing them into resonance.[14,108,109] In the phycobiliproteins, one of the vibrations is of special interest because of its potential influence on energy transfer in the regime where Förster theory breaks down due to slight delocalization of the excitation.[25] This is the topic of the next section.

**3.5. 1585 $cm^{-1}$ Mode.** The delocalization of vibrations across multiples chromophores is not expected for chromophores having weak electronic coupling between them. However, motivated by understanding the fastest energy-transfer step in PC645, which occurs over the largest energy jump in the protein, delocalization of the 1585 $cm^{-1}$ vibrational mode was investigated by Dean et al.[25] The study compared amplitude patterns of the mode in 2D electronic spectroscopy and theoretical models that support its role as a potential enhancer of energy-transfer rates. The screened coupling between DBV and PCB in PC645 is predicted to be 38 $cm^{-1}$[110] and the energy gap between their excited states is near-resonant with the 1585 $cm^{-1}$ oscillations (Figure 3D in ref 25). That is, the $v = 1$ state in the excited-state manifold of PCB (to be called $PCB_{v=1}$) is very close in energy to the $v = 0$ lower exciton state of DBV, thereby bridging the large energy gap by the vibrational ladder of the acceptor. Through 2D electronic spectroscopy amplitude patterns of the oscillations, it was determined that the 1585 $cm^{-1}$ mode had electronic character through mixing with the near-isoenergetic $DBV^-$ excited state. This coupling was shown to have the potential to enhance energy-transfer rates contributed by this pathway by up to 3.5-fold because of the enhanced transition strength of the acceptor, which increases the overlap integral between donor and acceptor states in Förster theory, and suggests a design principle for optimal light harvesting.

The work in the present study allows for additional characterization of the 1585 $cm^{-1}$ mode, which is dominantly present in all four proteins. Because each of the DOAS is characterized by an oscillation frequency with an associated dephasing time, it allows for comparative analysis of specific oscillations. Here, we will analyze the relative amplitudes of the 1585 $cm^{-1}$ mode across the four related proteins as a measure of vibronic intensity borrowing and explore its role in bridging donor and acceptor molecules by relating it to the corresponding energy-transfer rates and dephasing times. According to Figure 4 in ref 25, there is a marked dependence of the enhancement factor on the energy resonance between the donor and acceptor states. Because of the exciton splitting, which brings the $DBV^-$ closer in energy with the $PCB_{v=1}$ excited state, the closed structures fall into the resonance regime, whereas the open structures fall out.



DOI: 10.1021/acs.jpcb.8b02629
J. Phys. Chem. B 2018, 122, 6328−6340

Figure 6B plots the relative amplitudes based on the areas/$\gamma_n$ of the DOAS in each of the four proteins normalized to the respective areas/$\gamma_n$ of the 660 $cm^{-1}$ mode. The 660 $cm^{-1}$ mode is used as an internal standard because it is present in all four proteins. The area/$\gamma_n$ (mOD ps cm) is the integral over the probe frequency of the DOAS associated with oscillation $\nu$ (mOD/$cm^{-1}$) normalized by the dephasing rate of the mode ($ps^{-1}$). The closed structures possess greater relative amplitudes for the normalized 1585 $cm^{-1}$ mode than the open structures and these correlate with the energy-transfer rates from DBV to PCB in accord with the predictions from the vibronic coupling model suggested by Dean et al.[25] At last, we compare the relative dephasing rates in Figure 6B. Energy transfer, when predominantly incoherent is a dephasing mechanism and the reported vibrational dephasing rates of the 1585 $cm^{-1}$ mode correlate with the energy-transfer rates, exhibiting approximately twice the energy transfer rate, in each of the four proteins. Fast vibrational relaxation in PCB states may aid in dissipating the excess vibrational energy after energy transfer from DBV states.[82]

## 4. CONCLUSIONS

This analysis revealed a few dominant trends between the four phycobiliproteins. Although the accurate site energies are not clearly defined for all four proteins, they have similar absorption spectra and structures, which indicate that the energy ladders similarly involve high-energy DBV chromophores (≈580 nm) and lower-energy PCB chromophores (≈630 nm). Energy transfer initiated by the DBV chromophores occurs at the fastest rate and with the largest energy jump in all four structures. This rate is approximately twice as fast for the closed structures, having dimeric central DBV chromophores (distance ≈ 0.5 nm), as it is for the open structures, having weakly coupled DBV chromophores (distance ≈ 2 nm). The DOAS analysis allows for the simultaneous global time-domain fitting of vibrational frequencies present in the complexes. The DOAS are a read-out of the amplitude for a particular vibrational mode as a function of probe wavelength. Between 15 and 24 unique Franck−Condon-active vibrational modes with characteristic dephasing times were uncovered for the four phycobiliproteins, which based on their amplitude and phase characteristics can be assigned to excited-state vibrational oscillations. The lifetimes of the excited-state vibrations range from around 100 fs to over 1 ps and may exceed the lifetime of the first energy-transfer step.

Energetically bridging the donor and acceptor states is a 1585 $cm^{-1}$ mode, which was previously suggested to enhance the energy-transfer rates as a function of resonance between the states (DBV and $PCB_{0=1}$). We find that the extent of vibronic coupling between the donor and acceptor chromophores, as determined by relative amplitudes of the bridging 1585 $cm^{-1}$ mode across the set of four proteins, determines the rate (and thus efficiency) of down-conversion in the complexes. The closed structures, having exciton splitting in the central dimer, bring the donor and acceptors into closer resonance, according to the vibronic enhancement regime, than the open structures. This work provides additional evidence that this directed energy transfer between energetically disparate chromophores is a design principle used by cryptophytes.

## ■ ASSOCIATED CONTENT

### Supporting Information

The Supporting Information is available free of charge on the ACS Publications website at DOI: 10.1021/acs.jpcb.8b02629.

Selected time traces of PC577, PC612, PC630, and PC645 data; population dynamics and oscillation features at 580 nm; overview of the estimated DOAS and phases; and identified DOAS and their parameters from global fits (PDF)

## ■ AUTHOR INFORMATION


### Corresponding Author

*E-mail: gscholes@princeton.edu. Phone: 609-258-0729.

### ORCID

Chanelle C. Jumper: 0000-0002-0694-2758

Gregory D. Scholes: 0000-0003-3336-7960


### Author Contributions

‖C.C.J. and I.H.M.v.S. contributed equally to this work.

### Notes

The authors declare no competing financial interest.

## ■ ACKNOWLEDGMENTS

We thank Jacob Dean, Shahnawaz Rafiq, Rienk van Grondelle, and Pavel Malý for helpful discussions. G.D.S. acknowledges the Canadian Institute For Advanced Research (CIFAR). C.C.J. acknowledges funding for her doctoral studies from NSERC Canada Graduate Scholarships and the University of Toronto. I.H.M.v.S. acknowledges funding from the European Union's Horizon 2020 research and innovation programme under grant agreement no 654148 Laserlab-Europe. G.D.S. acknowledges the United States Air Force Office of Scientific Research (AFOSR) (FA9550-13-1-0005).

## ■ REFERENCES


(1) Blankenship, R. E. *Molecular Mechanisms of Photosynthesis*; World Sci.: London, 2002.

(2) Green, B. R.; Parson, W. W. *Light-Harvesting Antennas in Photosynthesis*; Kluwer: Dordrecht, 2003.

(3) Curutchet, C.; Kongsted, J.; Muñoz-Losa, A.; Hossein-Nejad, H.; Scholes, G. D.; Mennucci, B. Photosynthetic Light-Harvesting Is Tuned by the Heterogeneous Polarizable Environment of the Protein. *J. Am. Chem. Soc.* **2011**, *133*, 3078−3084.

(4) Abramavicius, D.; Valkunas, L. Role of Coherent Vibrations in Energy Transfer and Conversion in Photosynthetic Pigment−Protein Complexes. *Photosynth. Res.* **2016**, *127*, 33−47.

(5) Chin, A. W.; Prior, J.; Rosenbach, R.; Caycedo-Soler, F.; Huelga, S. F.; Plenio, M. B. The Role of Non-Equilibrium Vibrational Structures in Electronic Coherence and Recoherence in Pigment-Protein Complexes. *Nat. Phys.* **2013**, *9*, 113−118.

(6) Womick, J. M.; Moran, A. M. Vibronic Enhancement of Exciton Sizes and Energy Transport in Photosynthetic Complexes. *J. Phys. Chem. B* **2011**, *115*, 1347−1356.

(7) Chenu, A.; Christensson, N.; Kauffmann, H. F.; Mančal, T. Enhancement of Vibronic and Ground-State Vibrational Coherences in 2d Spectra of Photosynthetic Complexes. *Sci. Rep.* **2013**, *3*, 2029.

(8) Christensson, N.; Kauffmann, H. F.; Pullerits, T.; Mančal, T. Origin of Long-Lived Coherences in Light-Harvesting Complexes. *J. Phys. Chem. B* **2012**, *116*, 7449−7454.

(9) Lim, J.; Paleček, D.; Caycedo-Soler, F.; Lincoln, C. N.; Prior, J.; von Berlepsch, H.; Huelga, S. F.; Plenio, M. B.; Zigmantas, D.; Hauer, J. Vibronic Origin of Long-Lived Coherence in an Artificial Molecular Light Harvester. *Nat. Commun.* **2015**, *6*, 7755.




DOI: 10.1021/acs.jpcb.8b02629
J. Phys. Chem. B 2018, 122, 6328−6340

(10) Plenio, M. B.; Almeida, J.; Huelga, S. F. Origin of Long-Lived Oscillations in 2d-Spectra of a Quantum Vibronic Model: Electronic Versus Vibrational Coherence. *J. Chem. Phys.* **2013**, *139*, 235102.
(11) Womick, J. M.; West, B. A.; Scherer, N. F.; Moran, A. M. Vibronic Effects in the Spectroscopy and Dynamics of C-Phycocyanin. *J. Phys. B: At., Mol. Opt. Phys.* **2012**, *45*, 154016.
(12) Tiwari, V.; Peters, W. K.; Jonas, D. M. Electronic Resonance with Anticorrelated Pigment Vibrations Drives Photosynthetic Energy Transfer Outside the Adiabatic Framework. *Proc. Natl. Acad. Sci. U.S.A.* **2013**, *110*, 1203−1208.
(13) Novelli, F.; Nazir, A.; Richards, G. H.; Roozbeh, A.; Wilk, K. E.; Curmi, P. M. G.; Davis, J. A. Vibronic Resonances Facilitate Excited-State Coherence in Light-Harvesting Proteins at Room Temperature. *J. Phys. Chem. Lett.* **2015**, *6*, 4573−4580.
(14) Fuller, F. D.; Pan, J.; Gelzinis, A.; Butkus, V.; Senlik, S. S.; Wilcox, D. E.; Yocum, C. F.; Valkunas, L.; Abramavicius, D.; Ogilvie, J. P. Vibronic Coherence in Oxygenic Photosynthesis. *Nat. Chem.* **2014**, *6*, 706−711.
(15) Viani, L.; Corbella, M.; Curutchet, C.; O'Reilly, E. J.; Olaya-Castro, A.; Mennucci, B. Molecular Basis of the Exciton−Phonon Interactions in the Pe545 Light-Harvesting Complex. *Phys. Chem. Chem. Phys.* **2014**, *16*, 16302−16311.
(16) Kolli, A.; O'Reilly, E. J.; Scholes, G. D.; Olaya-Castro, A. The Fundamental Role of Quantized Vibrations in Coherent Light Harvesting by Cryptophyte Algae. *J. Chem. Phys.* **2012**, *137*, 174109.
(17) O'Reilly, E. J.; Olaya-Castro, A. Non-Classicality of the Molecular Vibrations Assisting Exciton Energy Transfer at Room Temperature. *Nat. Commun.* **2014**, *5*, 3012.
(18) Hein, B.; Kreisbeck, C.; Kramer, T.; Rodríguez, M. Modelling of Oscillations in Two-Dimensional Echo-Spectra of the Fenna−Matthews−Olson Complex. *New J. Phys.* **2012**, *14*, 023018.
(19) McClure, S. D.; Turner, D. B.; Arpin, P. C.; Mirkovic, T.; Scholes, G. D. Coherent Oscillations in the Pc577 Cryptophyte Antenna Occur in the Excited Electronic State. *J. Phys. Chem. B* **2014**, *118*, 1296−1308.
(20) Arpin, P. C.; et al. Spectroscopic Studies of Cryptophyte Light Harvesting Proteins: Vibrations and Coherent Oscillations. *J. Phys. Chem. B* **2015**, *119*, 10025−10034.
(21) Malý, P.; Somsen, O. J. G.; Novoderezhkin, V. I.; Mančal, T.; van Grondelle, R. The Role of Resonant Vibrations in Electronic Energy Transfer. *ChemPhysChem* **2016**, *17*, 1356−1368.
(22) Butkus, V.; Zigmantas, D.; Abramavicius, D.; Valkunas, L. Distinctive Character of Electronic and Vibrational Coherences in Disordered Molecular Aggregates. *Chem. Phys. Lett.* **2013**, *587*, 93−98.
(23) Dijkstra, A. G.; Wang, C.; Cao, J.; Fleming, G. R. Coherent Exciton Dynamics in the Presence of Underdamped Vibrations. *J. Phys. Chem. Lett.* **2015**, *6*, 627−632.
(24) Perlík, V.; Seibt, J.; Cranston, L. J.; Cogdell, R. J.; Lincoln, C. N.; Savolainen, J.; Šanda, F.; Mančal, T.; Hauer, J. Vibronic Coupling Explains the Ultrafast Carotenoid-to-Bacteriochlorophyll Energy Transfer in Natural and Artificial Light Harvesters. *J. Chem. Phys.* **2015**, *142*, 212434.
(25) Dean, J. C.; Mirkovic, T.; Toa, Z. S. D.; Oblinsky, D. G.; Scholes, G. D. Vibronic Enhancement of Algae Light Harvesting. *Chem* **2016**, *1*, 858−872.
(26) Fragnito, H. L.; Bigot, J.-Y.; Becker, P. C.; Shank, C. V. Evolution of the Vibronic Absorption Spectrum in a Molecule Following Impulsive Excitation with a 6 Fs Optical Pulse. *Chem. Phys. Lett.* **1989**, *160*, 101−104.
(27) Stock, G.; Domcke, W. Detection of Ultrafast Molecular-Excited-State Dynamics with Time- and Frequency-Resolved Pump-Probe Spectroscopy. *Phys. Rev. A: At., Mol., Opt. Phys.* **1992**, *45*, 3032−3040.
(28) Brazard, J.; Bizimana, L. A.; Gellen, T.; Carbery, W. P.; Turner, D. B. Experimental Detection of Branching at a Conical Intersection in a Highly Fluorescent Molecule. *J. Phys. Chem. Lett.* **2016**, *7*, 14−19.
(29) Cina, J. A.; Kovac, P. A.; Jumper, C. C.; Dean, J. C.; Scholes, G. D. Ultrafast Transient Absorption Revisited: Phase-Flips, Spectral Fingers, and Other Dynamical Features. *J. Chem. Phys.* **2016**, *144*, 175102.
(30) Dean, J. C.; Rafiq, S.; Oblinsky, D. G.; Cassette, E.; Jumper, C. C.; Scholes, G. D. Broadband Transient Absorption and Two-Dimensional Electronic Spectroscopy of Methylene Blue. *J. Phys. Chem. A* **2015**, *119*, 9098−9108.
(31) Rafiq, S.; Dean, J. C.; Scholes, G. D. Observing Vibrational Wavepackets During an Ultrafast Electron Transfer Reaction. *J. Phys. Chem. A* **2015**, *119*, 11837−11846.
(32) Rafiq, S.; Scholes, G. D. Slow Intramolecular Vibrational Relaxation Leads to Long-Lived Excited-State Wavepackets. *J. Phys. Chem. A* **2016**, *120*, 6792−6799.
(33) Wang, Q.; Schoenlein, R. W.; Peteanu, L. A.; Mathies, R. A.; Shank, C. V. Vibrationally Coherent Photochemistry in the Femtosecond Primary Event of Vision. *Science* **1994**, *266*, 422−424.
(34) Vos, M. H.; Jones, M. R.; Martin, J.-L. Vibrational Coherence in Bacterial Reaction Centers: Spectroscopic Characterisation of Motions Active During Primary Electron Transfer. *Chem. Phys.* **1998**, *233*, 179−190.
(35) Pollard, W. T.; Fragnito, H. L.; Bigot, J.-Y.; Shank, C. V.; Mathies, R. A. Quantum-Mechanical Theory for 6 Fs Dynamic Absorption Spectroscopy and Its Application to Nile Blue. *Chem. Phys. Lett.* **1990**, *168*, 239−245.
(36) Kumar, A. T. N.; Rosca, F.; Widom, A.; Champion, P. M. Investigations of Amplitude and Phase Excitation Profiles in Femtosecond Coherence Spectroscopy. *J. Chem. Phys.* **2001**, *114*, 701.
(37) Kumar, A. T. N.; Rosca, F.; Widom, A.; Champion, P. M. Investigations of Ultrafast Nuclear Response Induced by Resonant and Nonresonant Laser Pulses. *J. Chem. Phys.* **2001**, *114*, 6795−6815.
(38) De Silvestri, S.; Cerullo, G.; Lanzani, G. *Coherent Vibrational Dynamics*; CRC Press: Boca Raton, FL, 2008.
(39) Jonas, D. M.; Fleming, G. R. Vibrationally Abrupt Pulses in Pump-Probe Spectroscopy. In *Ultrafast Processes in Chemistry and Photobiology*; El-Sayed, M. A., Tanaka, I., Molin, Y., Eds.; Blackwell Scientific Publications: Oxford, U.K., 1995.
(40) Bardeen, C. J.; Wang, Q.; Shank, C. V. Femtosecond Chirped Pulse Excitation of Vibrational Wave Packets in Ld690 and Bacteriorhodopsin. *J. Phys. Chem. A* **1998**, *102*, 2759−2766.
(41) Bardeen, C. J.; Wang, Q.; Shank, C. V. Selective Excitation of Vibrational Wave Packet Motion Using Chirped Pulses. *Phys. Rev. Lett.* **1995**, *75*, 3410−3413.
(42) Jonas, D. M.; Bradforth, S. E.; Passino, S. A.; Fleming, G. R. Femtosecond Wavepacket Spectroscopy: Influence of Temperature, Wavelength, and Pulse Duration. *J. Phys. Chem.* **1995**, *99*, 2594−2608.
(43) Pollard, W. T.; Mathies, R. A. Analysis of Femtosecond Dynamic Absorption Spectra of Nonstationary States. *Annu. Rev. Phys. Chem.* **1992**, *43*, 497−523.
(44) Johnson, A. S.; Yuen-Zhou, J.; Aspuru-Guzik, A.; Krich, J. J. Practical Witness for Electronic Coherences. *J. Chem. Phys.* **2014**, *141*, 244109.
(45) Liebel, M.; Kukura, P. Broad-Band Impulsive Vibrational Spectroscopy of Excited Electronic States in the Time Domain. *J. Phys. Chem. Lett.* **2013**, *4*, 1358−1364.
(46) van Stokkum, I. H. M.; Jumper, C. C.; Snellenburg, J. J.; Scholes, G. D.; van Grondelle, R.; Malý, P. Estimation of Damped Oscillation Associated Spectra from Ultrafast Transient Absorption Spectra. *J. Chem. Phys.* **2016**, *145*, 174201.
(47) Schott, S.; Ress, L.; Hrušák, J.; Nuernberger, P.; Brixner, T. Identification of Photofragmentation Patterns in Trihalide Anions by Global Analysis of Vibrational Wavepacket Dynamics in Broadband Transient Absorption Data. *Phys. Chem. Chem. Phys.* **2016**, *18*, 33287−33302.
(48) Harrop, S. J.; Wilk, K. E.; Dinshaw, R.; Collini, E.; Mirkovic, T.; Teng, C. Y.; Oblinsky, D. G.; Green, B. R.; Hoef-Emden, K.; Hiller, R. G. Single-Residue Insertion Switches the Quaternary Structure and Exciton States of Cryptophyte Light-Harvesting Proteins. *Proc. Natl. Acad. Sci. U.S.A.* **2014**, *111*, E2666−E2675.


DOI: 10.1021/acs.jpcb.8b02629
*J. Phys. Chem. B* 2018, 122, 6328−6340

(49) van Stokkum, I. H. M.; Larsen, D. S.; van Grondelle, R. Erratum to "Global and Target Analysis of Time-Resolved Spectra". *Biochim. Biophys. Acta* **2004**, *1658*, 262.
(50) van Stokkum, I. H. M.; Larsen, D. S.; van Grondelle, R. Global and Target Analysis of Time-Resolved Spectra. *Biochim. Biophys. Acta* **2004**, *1657*, 82−104.
(51) Holzwarth, A. R. Data Analysis of Time-Resolved Measurements. In *Biophysical Techniques in Photosynthesis*; Amesz, J., Hoff, A. J., Eds.; Kluwer: Dordrecht, The Netherlands, 1996; pp 75−92.
(52) Mirkovic, T.; Doust, A. B.; Kim, J.; Wilk, K. E.; Curutchet, C.; Mennucci, B.; Cammi, R.; Curmi, P. M. G.; Scholes, G. D. Ultrafast Light Harvesting Dynamics in the Cryptophyte Phycocyanin 645. *Photochem. Photobiol.* **2007**, *6*, 964−975.
(53) Marin, A.; Doust, A. B.; Scholes, G. D.; Wilk, K. E.; Curmi, P. M. G.; van Stokkum, I. H. M.; van Grondelle, R. Flow of Excitation Energy in the Cryptophyte Light-Harvesting Antenna Phycocyanin 645. *Biophys. J.* **2011**, *101*, 1004−1013.
(54) van der Weij-De Wit, C. D.; Doust, A. B.; van Stokkum, I. H. M.; Dekker, J. P.; Wilk, K. E.; Curmi, P. M. G.; Scholes, G. D.; van Grondelle, R. How Energy Funnels from the Phycoerythrin Antenna Complex to Photosystem I and Photosystem Ii in Cryptophyte Rhodomonas Cs24 Cells. *J. Phys. Chem. B* **2006**, *110*, 25066−25073.
(55) van der Weij-De Wit, C. D.; Doust, A. B.; van Stokkum, I. H. M.; Dekker, J. P.; Wilk, K. E.; Curmi, P. M. G.; van Grondelle, R. Phycocyanin Sensitizes Both Photosystem I and Photosystem Ii in Cryptophyte Chroomonas Ccmp270 Cells. *Biophys. J.* **2008**, *94*, 2423−2433.
(56) Malak, H.; Maccoll, R. Picosecond Fluorescence from Phycocyanin 612. *Photochem. Photobiol.* **1991**, *53*, 367−370.
(57) Holzwarth, A. D.; Wendler, J.; Schaffner, K.; Sundström, V.; Sandström, A.; Gillbro, T. Picosecond Kinetics of Excited State Relaxation in Biliverdin Dimethyl Ester. *Isr. J. Chem.* **1983**, *23*, 223−231.
(58) Tasler, R.; Moises, T.; Frankenberg-Dinkel, N. Biochemical and Spectroscopic Characterization of the Bacterial Phytochrome of Pseudomonas Aeruginosa. *FEBS J.* **2005**, *272*, 1927−1936.
(59) Nagarajan, V.; Alden, R. G.; Williams, J. C.; Parson, W. W. Ultrafast Exciton Relaxation in the B850 Antenna Complex of Rhodobacter Sphaeroides. *Proc. Natl. Acad. Sci. U.S.A.* **1996**, *93*, 13774−13779.
(60) Dostál, J.; Mančal, T.; Augulis, R.; Vácha, F.; Pšenčík, J.; Zigmantas, D. Two-Dimensional Electronic Spectroscopy Reveals Ultrafast Energy Diffusion in Chlorosomes. *J. Am. Chem. Soc.* **2012**, *134*, 11611−11617.
(61) Anna, J. M.; Ostroumov, E. E.; Maghlaoui, K.; Barber, J.; Scholes, G. D. Two-Dimensional Electronic Spectroscopy Reveals Ultrafast Downhill Energy Transfer in Photosystem I Trimers of the Cyanobacterium Thermosynechococcus Elongatus. *J. Phys. Chem. Lett.* **2012**, *3*, 3677−3684.
(62) Fidler, A. F.; Singh, V. P.; Long, P. D.; Dahlberg, P. D.; Engel, G. S. Time Scales of Coherent Dynamics in the Light-Harvesting Complex 2 (Lh2) of Rhodobacter Sphaeroides. *J. Phys. Chem. Lett.* **2013**, *4*, 1404−1409.
(63) Myers, J. A.; Lewis, K. L. M.; Fuller, F. D.; Tekavec, P. F.; Yocum, C. F.; Ogilvie, J. P. Two-Dimensional Electronic Spectroscopy of the D1-D2-Cyt B559 Photosystem Ii Reaction Center Complex. *J. Phys. Chem. Lett.* **2010**, *1*, 2774−2780.
(64) Schlau-Cohen, G. S.; Calhoun, T. R.; Ginsberg, N. S.; Read, E. L.; Ballottari, M.; Bassi, R.; van Grondelle, R.; Fleming, G. R. Pathways of Energy Flow in Lhcii from Two-Dimensional Electronic Spectroscopy. *J. Phys. Chem. B* **2009**, *113*, 15352−15363.
(65) Womick, J. M.; Moran, A. M. Exciton Coherence and Energy Transport in the Light-Harvesting Dimers of Allophycocyanin. *J. Phys. Chem. B* **2009**, *113*, 15747−15759.
(66) Zigmantas, D.; Read, E. L.; Mancal, T.; Brixner, T.; Gardiner, A. T.; Cogdell, R. J.; Fleming, G. R. Two-Dimensional Electronic Spectroscopy of the B800-B820 Light-Harvesting Complex. *Proc. Natl. Acad. Sci. U.S.A.* **2006**, *103*, 12672−12677.
(67) van Grondelle, R.; Novoderezhkin, V. I. Energy Transfer in Photosynthesis: Experimental Insights and Quantitative Models. *Phys. Chem. Chem. Phys.* **2006**, *8*, 793−807.
(68) Edington, M. D.; Riter, R. E.; Beck, W. F. Interexciton-State Relaxation and Exciton Localization in Allophycocyanin Trimers. *J. Phys. Chem.* **1996**, *100*, 14206−14217.
(69) van Grondelle, R.; Novoderezhkin, V. Dynamics of Excitation Energy Transfer in the Lh1 and Lh2 Light-Harvesting Complexes of Photosynthetic Bacteria. *Biochemistry* **2001**, *40*, 15057−15068.
(70) Dahlberg, P. D.; Ting, P.-C.; Massey, S. C.; Martin, E. C.; Hunter, C. N.; Engel, G. S. Electronic Structure and Dynamics of Higher-Lying Excited States in Light Harvesting Complex 1 from Rhodobacter Sphaeroides. *J. Phys. Chem. A* **2016**, *120*, 4124−4130.
(71) Arnett, D. C.; Moser, C. C.; Dutton, P. L.; Scherer, N. F. The First Events in Photosynthesis: Electronic Coupling and Energy Transfer Dynamics in the Photosynthetic Reaction Center from Rhodobacter Sphaeroides. *J. Phys. Chem. B* **1999**, *103*, 2014−2032.
(72) Homoelle, B. J.; Edington, M. D.; Diffey, W. M.; Beck, W. F. Stimulated Photon-Echo and Transient-Grating Studies of Protein-Matrix Solvation Dynamics and Interexciton-State Radiationless Decay in A Phycocyanin and Allophycocyanin. *J. Phys. Chem. B* **1998**, *102*, 3044−3052.
(73) Roscioli, J. D.; Ghosh, S.; LaFountain, A. M.; Frank, H. A.; Beck, W. F. Quantum Coherent Excitation Energy Transfer by Carotenoids in Photosynthetic Light Harvesting. *J. Phys. Chem. Lett.* **2017**, *8*, 5141−5147.
(74) Jumper, C. C.; Anna, J. M.; Stradomska, A.; Schins, J.; Myahkostupov, M.; Prusakova, V.; Oblinsky, D. G.; Castellano, F. N.; Knoester, J.; Scholes, G. D. Intramolecular Radiationless Transitions Dominate Exciton Relaxation Dynamics. *Chem. Phys. Lett.* **2014**, *599*, 23−33.
(75) Wand, A.; Kallush, S.; Shoshanim, O.; Bismuth, O.; Kosloff, R.; Ruhman, S. Chirp Effects on Impulsive Vibrational Spectroscopy: A Multimode Perspective. *Phys. Chem. Chem. Phys.* **2010**, *12*, 2149−2163.
(76) Polli, D.; Lüer, L.; Cerullo, G. High-Time-Resolution Pump-Probe System with Broadband Detection for the Study of Time-Domain Vibrational Dynamics. *Rev. Sci. Instrum.* **2007**, *78*, 103108.
(77) Horikoshi, K.; Misawa, K.; Lang, R. Rapid Motion Capture of Mode-Specific Quantum Wave Packets Selectively Generated by Phase-Controlled Optical Pulses. *J. Chem. Phys.* **2007**, *127*, 054104.
(78) Florean, A. C.; Carroll, E. C.; Spears, K. G.; Sension, R. J.; Bucksbaum, P. H. Optical Control of Excited-State Vibrational Coherences of a Molecule in Solution: The Influence of the Excitation Pulse Spectrum and Phase in Ld690. *J. Phys. Chem. B* **2006**, *110*, 20023−20031.
(79) Lanzani, G.; Zavelani-Rossi, M.; Cerullo, G.; Comoretto, D.; Dellepiane, G. Real-Time Observation of Coherent Nuclear Motion in Polydiacetylene Isolated Chains. *Phys. Rev. B: Condens. Matter Mater. Phys.* **2004**, *69*, 134302.
(80) Vos, M. H.; Rappaport, F.; Lambry, J.-C.; Breton, J.; Martin, J.-L. Visualization of Coherent Nuclear Motion in a Membrane Protein by Femtosecond Spectroscopy. *Nature* **1993**, *363*, 320.
(81) Jumper, C. C.; Arpin, P. C.; Turner, D. B.; McClure, S. D.; Rafiq, S.; Dean, J. C.; Cina, J. A.; Kovac, P. A.; Mirkovic, T.; Scholes, G. D. Broad-Band Pump−Probe Spectroscopy Quantifies Ultrafast Solvation Dynamics of Proteins and Molecules. *J. Phys. Chem. Lett.* **2016**, *7*, 4722−4731.
(82) Blau, S. M.; Bennett, D. I. G.; Kreisbeck, C.; Scholes, G. D.; Aspuru-Guzik, A. Local Protein Solvation Drives Direct Down-Conversion in Phycobiliprotein Pc645 Via Incoherent Vibronic Transport. *Proc. Natl. Acad. Sci. U.S.A.* **2018**, *115*, E3342−E3350.
(83) Scherer, N. F.; Ziegler, L. D.; Fleming, G. R. Heterodyne-Detected Time-Domain Measurement of I2 Predissociation and Vibrational Dynamics in Solution. *J. Chem. Phys.* **1992**, *96*, 5544−5547.
(84) Vos, M. H.; Lambry, J. C.; Robles, S. J.; Youvan, D. C.; Breton, J.; Martin, J. L. Direct Observation of Vibrational Coherence in


DOI: 10.1021/acs.jpcb.8b02629
J. Phys. Chem. B 2018, 122, 6328−6340

Bacterial Reaction Centers Using Femtosecond Absorption Spectroscopy. *Proc. Natl. Acad. Sci. U.S.A.* **1991**, *88*, 8885−8889.
(85) Vos, M. H.; Martin, J.-L. Femtosecond Processes in Proteins. *Biochim. Biophys. Acta* **1999**, *1411*, 1−20.
(86) Kneip, C.; Parbel, A.; Foerstendorf, H.; Scheer, H.; Siebert, F.; Hildebrandt, P. Fourier Transform near-Infrared Resonance Raman Spectroscopic Study of the A-Subunit of Phycoerythrocyanin and Phycocyanin from the Cyanobacterium Mastigocladus Laminosus. *J. Raman Spectrosc.* **1998**, *29*, 939−944.
(87) Andel, F.; Murphy, J. T.; Haas, J. A.; McDowell, M. T.; van der Hoef, I.; Lugtenburg, J.; Lagarias, J. C.; Mathies, R. A. Probing the Photoreaction Mechanism of Phytochrome through Analysis of Resonance Raman Vibrational Spectra of Recombinant Analogues. *Biochemistry* **2000**, *39*, 2667−2676.
(88) Vos, M. H.; Jones, M. R.; Hunter, C. N.; Breton, J.; Lambry, J.-C.; Martin, J.-L. Coherent Dynamics During the Primary Electron-Transfer Reaction in Membrane-Bound Reaction Centers of Rhodobacter Sphaeroides. *Biochemistry* **1994**, *33*, 6750−6757.
(89) Stanley, R. J.; Boxer, S. G. Oscillations in the Spontaneous Fluorescence from Photosynthetic Reaction Centers. *J. Phys. Chem.* **1995**, *99*, 859−863.
(90) Chachisvilis, M.; Pullerits, T.; Jones, M. R.; Hunter, C. N.; Sundström, V. Vibrational Dynamics in the Light-Harvesting Complexes of the Photosynthetic Bacterium Rhodobacter Sphaeroides. *Chem. Phys. Lett.* **1994**, *224*, 345−354.
(91) Vos, M. H.; Jones, M. R.; Hunter, C. N.; Breton, J.; Martin, J. L. Coherent Nuclear Dynamics at Room Temperature in Bacterial Reaction Centers. *Proc. Natl. Acad. Sci. U.S.A.* **1994**, *91*, 12701−12705.
(92) Chachisvilis, M.; Sundström, V. Femtosecond Vibrational Dynamics and Relaxation in the Core Light-Harvesting Complex of Photosynthetic Purple Bacteria. *Chem. Phys. Lett.* **1996**, *261*, 165−174.
(93) Bradforth, S. E.; Jimenez, R.; van Mourik, F.; van Grondelle, R.; Fleming, G. R. Excitation Transfer in the Core Light-Harvesting Complex (Lh-1) of Rhodobacter Sphaeroides: An Ultrafast Fluorescence Depolarization and Annihilation Study. *J. Phys. Chem.* **1995**, *99*, 16179−16191.
(94) Kumble, R.; Palese, S.; Visschers, R. W.; Dutton, P. L.; Hochstrasser, R. M. Ultrafast Dynamics within the B820 Subunit from the Core (Lh-1) Antenna Complex of Rs. Rubrum. *Chem. Phys. Lett.* **1996**, *261*, 396−404.
(95) Diffey, W. M.; Homoelle, B. J.; Edington, M. D.; Beck, W. F. Excited-State Vibrational Coherence and Anisotropy Decay in the Bacteriochlorophyll a Dimer Protein B820. *J. Phys. Chem. B* **1998**, *102*, 2776−2786.
(96) Shelly, K. R.; Carson, E. A.; Beck, W. F. Vibrational Coherence from the Dipyridine Complex of Bacteriochlorophyll A: Intramolecular Modes in the 10−220-Cm-1 Regime, Intermolecular Solvent Modes, and Relevance to Photosynthesis. *J. Am. Chem. Soc.* **2003**, *125*, 11810−11811.
(97) Joo, T.; Jia, Y.; Yu, J.-Y.; Jonas, D. M.; Fleming, G. R. Dynamics in Isolated Bacterial Light Harvesting Antenna (Lh2) of Rhodobacter Sphaeroides at Room Temperature. *J. Phys. Chem.* **1996**, *100*, 2399−2409.
(98) Savikhin, S.; Zhu, Y.; Lin, S.; Blankenship, R. E.; Struve, W. S. Femtosecond Spectroscopy of Chlorosome Antennas from the Green Photosynthetic Bacterium Chloroflexus Aurantiacus. *J. Phys. Chem.* **1994**, *98*, 10322−10334.
(99) Savikhin, S.; Struve, W. S. Low-Temperature Energy Transfer in Fmo Trimers from the Green Photosynthetic Bacterium Chlorobium Tepidum. *Photosynth. Res.* **1996**, *48*, 271−276.
(100) Rätsep, M.; Freiberg, A. Electron−Phonon and Vibronic Couplings in the Fmo Bacteriochlorophyll a Antenna Complex Studied by Difference Fluorescence Line Narrowing. *J. Lumin.* **2007**, *127*, 251−259.
(101) Wendling, M.; Pullerits, T.; Przyjalgowski, M. A.; Vulto, S. I. E.; Aartsma, T. J.; van Grondelle, R.; van Amerongen, H. Electron−Vibrational Coupling in the Fenna−Matthews−Olson Complex of Prosthecochloris Aestuarii Determined by Temperature-Dependent Absorption and Fluorescence Line-Narrowing Measurements. *J. Phys. Chem. B* **2000**, *104*, 5825−5831.
(102) Maiuri, M.; Ostroumov, E. E.; Saer, R. G.; Blankenship, R. E.; Scholes, G. D. Coherent Wavepackets in the Fenna−Matthews−Olson Complex Are Robust to Excitonic-Structure Perturbations Caused by Mutagenesis. *Nat. Chem.* **2018**, *10*, 177.
(103) Panitchayangkoon, G.; Hayes, D.; Fransted, K. A.; Caram, J. R.; Harel, E.; Wen, J.; Blankenship, R. E.; Engel, G. S. Long-Lived Quantum Coherence in Photosynthetic Complexes at Physiological Temperature. *Proc. Natl. Acad. Sci. U.S.A.* **2010**, *107*, 12766−12770.
(104) Book, L. D.; Arnett, D. C.; Hu, H.; Scherer, N. F. Ultrafast Pump−Probe Studies of Excited-State Charge-Transfer Dynamics in Blue Copper Proteins. *J. Phys. Chem. A* **1998**, *102*, 4350−4359.
(105) Olbrich, C.; Strümpfer, J.; Schulten, K.; Kleinekathöfer, U. Theory and Simulation of the Environmental Effects on Fmo Electronic Transitions. *J. Phys. Chem. Lett.* **2011**, *2*, 1771−1776.
(106) Shim, S.; Rebentrost, P.; Valleau, S.; Aspuru-Guzik, A. Atomistic Study of the Long-Lived Quantum Coherences in the Fenna-Matthews-Olson Complex. *Biophys. J.* **2012**, *102*, 649−660.
(107) Lee, M. K.; Bravaya, K. B.; Coker, D. F. First Principles Models for Biological Light-Harvesting: Phycobiliprotein Complexes from Cryptophyte Algae. *J. Am. Chem. Soc.* **2017**, *139*, 7803−7814.
(108) Novoderezhkin, V. I.; Romero, E.; Prior, J.; van Grondelle, R. Exciton-Vibrational Resonance and Dynamics of Charge Separation in the Photosystem Ii Reaction Center. *Phys. Chem. Chem. Phys.* **2017**, *19*, 5195−5208.
(109) Romero, E.; Augulis, R.; Novoderezhkin, V. I.; Ferretti, M.; Thieme, J.; Zigmantas, D.; van Grondelle, R. Quantum Coherence in Photosynthesis for Efficient Solar Energy Conversion. *Nat. Phys.* **2014**, *10*, 676−682.
(110) Curutchet, C.; Scholes, G. D.; Mennucci, B.; Cammi, R. How Solvent Controls Electronic Energy Transfer and Light Harvesting: Toward a Quantum-Mechanical Description of Reaction Field and Screening Effects. *J. Phys. Chem. B* **2007**, *111*, 13253−13265.


DOI: 10.1021/acs.jpcb.8b02629
*J. Phys. Chem. B* 2018, 122, 6328−6340